A&A 452, 25–35 (2006)
DOI: 10.1051/0004-6361:20054283

Astronomy & Astrophysics

Time delay of SBS 0909+532

A. Ullán[1], L. J. Goicoechea[1], A. P. Zheleznyak[2], E. Koptelova[3], V. V. Bruevich[3], T. Akhunov[4], and O. Burkhonov[4]

[1] Departamento de Física Moderna, Universidad de Cantabria, Avda. de Los Castros s/n, 39005 Santander, Spain
e-mail: aurora.ullan@postgrado.unican.es; goicol@unican.es
[2] Institute of Astronomy of Kharkov National University, Sumskaya 35, 61022 Kharkov, Ukraine
e-mail: zheleznyak@astron.kharkov.ua
[3] Sternberg Astronomical Institute, Universitetski Pr. 13, 119992 Moscow, Russia
e-mail: koptelova@xray.sai.msu.ru; bruevich@sai.msu.ru
[4] Ulug Beg Astronomical Institute of Uzbek Academy of Science, Astronomicheskaya. Str. 33, 700052 Tashkent, Republic of Uzbekistan
e-mail: talat77@rambler.ru; boa@astrin.uzsci.net

Received 30 September 2005 / Accepted 12 January 2006

ABSTRACT

Aims. The time delays between the components of a lensed quasar are basic tools for analysing the expansion of the Universe and the structure of the main lens galaxy halo. In this paper, we focus on the variability and time delay of the double system SBS 0909+532A,B as well as the time behaviour of the field stars.

Methods. We use *VR* optical observations of SBS 0909+532A, B and the field stars in 2003. The frames were taken at Calar Alto, Maidanak, and Wise observatories, and the *VR* light curves of the field stars and quasar components were derived from aperture and point-spread function fitting methods. We measured the *R*-band time delay of the system from the χ^2 and dispersion techniques and 1000 synthetic light curves based on the observed records.

Results. One nearby field star (SBS 0909+532c) was found to be variable, and the other two nearby field stars are non-variable sources. With respect to the quasar components, the *R*-band records seem more reliable and are more densely populated than the *V*-band ones. The observed *R*-band fluctuations permit a pre-conditioned measurement of the time delay. From the χ^2 minimization, if we assume that the quasar emission is observed first in B and afterwards in A (in agreement with basic observations of the system and the corresponding predictions), we obtain $\Delta\tau_{\rm BA} = -45^{+1}_{-11}$ days (95% confidence interval). The dispersion technique leads to a similar delay range. A by-product of the analysis is the determination of a totally corrected flux ratio in the *R* band (corrected by the time delay and the contamination due to the galaxy light). Our 95% measurement $\Delta m_{\rm BA} = m_{\rm B}(t + \Delta\tau_{\rm BA}) - m_{\rm A}(t) = 0.575 \pm 0.014$ mag is in excellent agreement with previous results from contaminated fluxes at the same time of observation.

Key words. gravitational lensing – galaxies: quasars: general – galaxies: quasars: individual: SBS 0909+532 – stars: variables: general

1. Introduction

The system SBS 0909+532 was discovered by Stepanyan et al. (1991). Some years later, a collaboration between the Hamburger Sternwarte and the Harvard-Smithsonian Center for Astrophysics resolved the system into a pair of quasars (A and B) with a direct *R*-band flux ratio (at the same time of observation) $\Delta m = m_{\rm B} - m_{\rm A} = 0.58$ mag and a separation of about 1.″1 (Kochanek et al. 1997). The direct *R*-band flux ratio was not consistent with the direct flux ratios at other wavelengths: $\Delta m = 0.31$ mag in the *I* band and $\Delta m = 1.29$ mag in the *B* band. From observations with the 4.2 m William Herschel Telescope, a Spanish collaboration got spectra for each component of the system. The data showed that the system consists of two quasars with the same redshift ($z_{\rm s} = 1.377$) and identical spectral distribution, supporting the gravitational lens interpretation of SBS 0909+532 (Oscoz et al. 1997). Oscoz et al. (1997) detected an Mg II doublet in absorption at the same redshift ($z_{\rm abs} = 0.83$) in both components, and they suggested that the absorption features were associated with the photometrically unidentified lensing galaxy. Through a singular isothermal sphere (SIS) lens model, the authors also inferred the first constraint on the time delay between the components: $|\Delta\tau_{\rm BA}| \leq 140$ days, where $\Delta\tau_{\rm BA}$ is the delay of B with respect to A, and the Hubble constant is assumed to be $H_0 = 70\ {\rm km\,s^{-1}\,Mpc^{-1}}$.

In recent years, Lubin et al. (2000) have indicated the possible nature of the main deflector (early-type galaxy) and confirmed its redshift ($z_{\rm d} = 0.830$). Lehár et al. (2000) reported on a program including Hubble Space Telescope (HST) observations of SBS 0909+532. They discovered the main lens galaxy between the components, which has a large effective radius, with a correspondingly low surface brightness. This lens galaxy is closer to the brightest component (A), which does not contradict SIS-like lens models when the farther and fainter component (B) is more strongly affected by dust extinction (see below). The colours of the lens are consistent with those of an early-type galaxy at redshift 0.83. Assuming a singular isothermal ellipsoid (SIE) model, Lehár et al. predicted a time delay $\Delta\tau_{\rm BA}$ in the range $[-10, -87]$ days ($H_0 = 70\ {\rm km\,s^{-1}\,Mpc^{-1}}$). At a given emission time, the sign "–" means that the corresponding signal is observed first in B and later in A. The COSMOGRAIL collaboration has provided the distribution of predicted time delays of the system (Saha et al. 2006). In their histogram (Fig. 10 of Saha et al.), there are two features: the main feature is an asymmetric peak around − 80 days and the secondary one is another asymmetric peak around −45 days. Therefore, if the COSMOGRAIL

predictions are right, the time delay is very probably 2−3 months (component B leading component A), but we cannot rule out a delay of about one and a half months. On the other hand, the flux ratio anomaly pointed by Kochanek et al. (1997) was confirmed and accurately studied by Motta et al. (2002) and Mediavilla et al. (2005), who reported the existence of differential extinction in the main lens galaxy. Chartas (2000) and Page et al. (2004) also studied the system in the X-ray domain.

Time delays are basic tools for discussing the present expansion rate of the Universe and the structure of the main lens galaxy haloes (e.g., Refsdal 1964; Kochanek et al. 2004), so that variability studies are crucial. While some time delays have been measured from radio light curves (PKS 1830−211: Lovell et al. 1998; Q0957+561: Haarsma et al. 1999; B0218+357: Biggs et al. 1999; B1600+434: Koopmans et al. 2000; B1422+231: Patnaik & Narasimha 2001; B1608+656: Fassnacht et al. 2002) or X-ray variability (e.g., Q2237+0305: Dai et al. 2003), an important set of delays is based on optical monitoring of gravitationally lensed quasars. Optical frames taken at Apache Point Observatory, Fred Lawrence Whipple Observatory, and Teide Observatory were used to estimate a 14-month delay for the double system Q0957+561 (e.g., Pelt et al. 1996; Kundić et al. 1997; Serra-Ricart et al. 1999; Ovaldsen et al. 2003). Although the time delay of this first multiple quasar has been confirmed through independent observations, the measurement is only 5% accurate, or equivalently, there is an uncertainty of about 20 days (Goicoechea 2002). The Tel-Aviv University (TAU) group have recently determined the time delay between the two components of HE 1104−1805 (Ofek & Maoz 2003). The TAU delay of HE 1104−1805 disagrees with the earlier estimation by Gil-Merino et al. (2002), but it is in excellent agreement with the determination by Wyrzykowski et al. (2003). Schechter et al. (1997) measured two delays for the quadruply imaged quasar PG 1115+080. The Belgian-Nordic collaboration were intensely active during the past five years. They participated in several monitoring projects and measured several time delays at optical wavelengths: B1600+434 (Burud et al. 2000), HE 2149−2745 (Burud et al. 2002a), RXJ 0911.4+0551 (Hjorth et al. 2002), SBS 1520+530 (Burud et al. 2002b), and FBQ 0951+2635 (Jakobsson et al. 2005). The formal accuracies of these 5 estimations range from 5 to 25% (the 1σ error bars vary from 4 to 24 days). Kochanek et al. (2005) also measured the time delays between the components of the quadruple quasar HE 0435−1223.

The aim of this paper is to present *VR* observations of SBS 0909+532 in 2003 conducted by the University of Cantabria (UC, Spain), the Institute of Astronomy of Kharkov National University (IAKhNU, Ukraine), the Sternberg Astronomical Institute (SAI, Russia), and the Ulug Beg Astronomical Institute of Uzbek Academy of Science (UBAI, Uzbekistan). We also present TAU observations of the field stars in 2003, which have been kindly made available to us. This new optical monitoring campaign was carried out at the Calar Alto Observatory (Spain), the Maidanak Observatory (Uzbekistan), and the Wise Observatory (Israel), and the frames were taken with the 1.5 m Spanish telescope, the 1.5 m AZT-22 telescope at Mt. Maidanak, and the Wise Observatory 1 m telescope (Sect. 2). In Sect. 3, we describe the methodology for obtaining the fluxes of the quasar components and the field stars. The *VR* light curves are also shown in Sect. 3. Section 4 is devoted to the time delay estimation from the light curves of A and B (quasar components) in the *R* band. Finally, in Sect. 5 we summarise our conclusions and discuss the feasibility of accurately determining the cosmic expansion rate and the surface density in the main lensing galaxy.

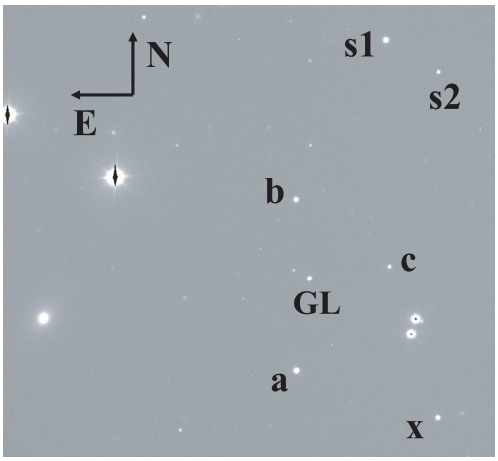

Fig. 1. Calar Alto image of SBS 0909+532, showing an FOV of ∼7′×7′. The field contains the gravitationally lensed quasar ("GL") and six bright and non-saturated stars ("a−c", "s1−s2" and "x"). The nearby ("a−c") and relatively far ("s1−s2") field stars were introduced by Kochanek et al. (1997) and Nakos et al. (2003), respectively. A sixth field star ("x") is also included in the FOV.

2. Observations

We have three different sets of frames for SBS 0909+532. The first set of optical frames covers the period between March 4 and June 2, 2003, and they are part of a UC project to test the feasibility of quasar monitoring programs through 1−2 m telescopes in Spain (Ullán 2005). These observations were made with the 1.52 m Spanish telescope at Calar Alto Observatory (EOCA), Almeria, Spain (see Ziad et al. 2005, for a site-testing on Calar Alto). The EOCA is equipped with a Tektronics 1024 × 1024 CCD detector, which has pixels with a physical size of 24 μm, giving a 0.4 arcsec pixel^{-1} angular scale. The gain is 6.55 e$^-$/ADU and the readout noise is 6.384 e$^-$. During this first monitoring, exposures in the *V* and *R* Johnson-Cousins filters were taken every night when clear, which makes a total of 20 observing nights. Bad weather in March and April 2003 prevented us from achieving a very dense sampling. For each monitoring night we had three consecutive frames on each filter, i.e., three 300 s exposures in the *V* passband and three 180 s exposures in the *R* passband. Those were the maximum exposure times to avoid saturation of selected stars in the field. In Fig. 1 we show a typical frame. In this typical exposure, half a dozen bright and non-saturated stars were fitted within the field of view (FOV). Following the notation of Kochanek et al. (1997), the FOV included the gravitationally lensed quasar ("GL") and nearby field stars "a" (South), "b" (North), and "c" (West). The FOV also included two stars that were introduced by Nakos et al. (2003) and were labeled as "s1" and "s2". These two stars are placed relatively far from the gravitational lens system, and they appear close to the NW edge of the frame (see Fig. 1). A sixth star ("x") appears close to the SW edge of the typical frame.

The second set of observations include frames in February 2003, as well as during April−May and October−November 2003. The total number of nights is 18. In this second program the images were taken with the 1.5 m AZT-22 telescope at Maidanak Observatory (Uzbekistan), with near diffraction-limited optics and careful thermo-stabilization, which allowed for high-angular-resolution imaging. The AZT-22 telescope

Table 1. Observations of SBS 0909+532 in 2003.

Observatory (telescope)	Frames/night (filter)	Observation periods
Calar Alto (1.5 m)	3×300 s (V) + 3×180 s (R)	March–June
Maidanak (1.5 m)	(3–11) $\times$ 180 s (R)	February, April–May, October–November
Wise (1.0 m)	1×420 s (R)	22 unevenly distributed nights

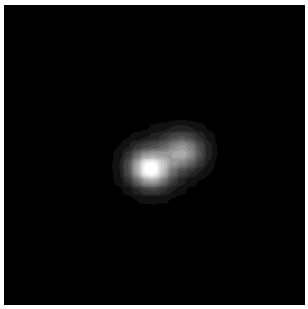

Fig. 2. Maidanak zoomed-in image of SBS 0909+532 (about 8″ on a side). We chose one of the frames taken with the best seeing conditions, and then expanded the portion occupied by the two quasar components A (the brightest object) and B (the faintest object), i.e., the GL in Fig. 1. To avoid the pixellation effect when a subframe is expanded, the brightness distribution is also smoothed.

has a LN-cooled (liquid nitrogen cooled) CCD-camera, SITe-005 CCD, manufactured in Copenhagen (Denmark). For this camera, the imaging area is split into 2000×800 pixel, where the pixel size is 15 μm and the intrinsic angular scale is 0.26 arcsec pixel^{-1}. The frames were taken in the R Bessel filter, which corresponds approximately to the R Johnson-Cousins passband. The poor tracking system of this telescope allows exposures only up to 3 min. To obtain sufficiently high photometric accuracy, we took several frames each observation night. With respect to the rectangular FOV of the telescope, the North/South coverage was 2.5 times smaller than the East/West one, so the "s1", "s2", and "x" stars were not included within the FOV. Figure 2 shows a zoomed-in image made from one of the best frames in terms of seeing. There are two close quasar components, but the very faint galaxy is not apparent. The observations at Mt. Maidanak are part of IAKhNU, SAI, and UBAI projects to follow up on the variability of gravitationally lensed quasars.

For the past six years, the TAU group has been monitoring several gravitationally lensed quasars with the Wise Observatory 1 m telescope. The targets are mainly monitored in the Johnson-Cousins R-band, and the frames obtained with a cryogenically cooled Tektronix 1024×1024-pixel back-illuminated CCD. The angular scale is 0.7 arcsec per pixel. This pixel scale and the median seeing ($FWHM$) of about 2″ do not allow resolving most of the lensed objects, e.g., SBS 0909+532. However, the frames of SBS 0909+532 in 2003 are characterized by wide FOVs, which incorporate the "a−c", "s1−s2", and "x" stars. This fact permits differential photometry between several pairs of field stars to be done, and thus the reliability of the Calar Alto and Maidanak records to be tested.

The pre-processing of the images included the usual bias subtraction, flat fielding using sky flats, sky subtraction, and cosmic-ray removal by using the Image Reduction and Analysis Facility (IRAF) and Munich Image Data Analysis System (MIDAS) environments. Some details about the whole observational campaign are included in Table 1 (observatories, telescopes, frames/night, filters, and observation periods).

3. Photometry and *VR* light curves

Due to the small angular separation between the two lensed components, about 1.″1 (Kochanek et al. 1997), the photometry of SBS 0909+532 is a difficult task. This task is also complicated by the presence of the main lensing galaxy between the components, which could make the computation of individual fluxes even harder. In general, aperture photometry does not work, so we must look for better approaches. An initial issue is to decide whether to include a photometric model for the lensing galaxy. In principle, when computing the fluxes of SBS 0909+532, we may use a galaxy model derived from the HST images of the system. The galaxy model could also be inferred from the best images in terms of seeing. Once the relevant information on the galaxy is known, we apply a PSF fitting method to all optical images, setting the galaxy properties to those derived from the HST or the best-quality images, and allowing the remaining parameters to vary (e.g., McLeod et al. 1998; Ullán et al. 2003).

Magain et al. (1998) also presented an alternative task (deconvolution) that combines all the frames obtained at different epochs to determine the numerical light distribution of the lensing galaxy, as well as the positions of the point-like sources (quasar components), since these parameters do not vary with time. The flux of the point-like sources are allowed to vary from image to image, which produces the light curves. However, these and other procedures have a reasonable limitation: they only work well when the galaxy light makes a significant contribution to the crowded regions in the individual frames. For a very faint galaxy in a standard (i.e., not superb) frame, there is confusion between galaxy signal and noise, so the use of a given galaxy model could lead to biased fluxes of the components. The biases will depend on the quality of the image (seeing, signal-to-noise ratio, etc.), which must produce artificial variability superposed on the real one. On the other hand, the use of a direct PSF fitting method (neglecting the galaxy brightness) leads to contaminated fluxes of the components. But if the galaxy is very faint, the contaminations will be small. Moreover, the variation of the quasar fluxes, seeing conditions, etc., will cause fluctuations in the contaminations, which are expected to be below the typical contamination levels. For standard frames of a quasar lensed by a very faint extended object, it is really difficult to choose between the approaches with and without galaxy.

Most of the Calar Alto and Maidanak individual frames of SBS 0909+532 do not show evidence of a galaxy brightness profile. This is due to the faintness of the galaxy, as we corroborate below. If we consider a hypothetical astronomer who neglects the galaxy brightness and does direct PSF fitting without taking the galaxy into account when computing the fluxes, it is possible to roughly estimate the maximum contamination from the galaxy to the closest component A (at 0.″4 from the centre of the deflector). We take the paper about 10 lens systems by Lehár et al. (2000) into account, where, in Table 3, we can find the best available photometric and astrometric (HST) data for SBS 0909+532. The authors were able to trace the galaxy light in the H passband by measuring its position and brightness. If we use the colours in the same table, we conclude that $m_{\rm gal} \sim 19$ mag and $m_{\rm A} \sim 16$ mag in the I band (near-IR), and

that $m_{\rm gal} > 20.4$ mag and $m_{\rm A} \sim 16.7$ mag in the V optical band. Therefore, as the R filter is placed just between the I filter and the V one, we may assume that $m_{\rm gal} - m_{\rm A} \sim 3.5$ mag in the R band. The difference of 3.5 mag is consistent with a ratio of fluxes $F_{\rm gal}/F_{\rm A}$ of about 1/25. Thus, in the case of QSO 0957+561, we found a R-band ratio of fluxes $F_{\rm gal}/F_{\rm A}$ of about 1/2.5 (Ullán et al. 2003), and now we have $F_{\rm gal}/F_{\rm A} \sim 1/25$, which explains our unsuccessful efforts when measuring the flux of the lens galaxy in standard frames.

As a result of that, in an extreme case (when direct PSF fitting leads to a magnitude $m_{\rm A+gal}$ instead of $m_{\rm A}$, i.e., all the galaxy light is included in the profile of the A component), we find a relationship: $m_{\rm A} = m_{\rm A+gal} + F_{\rm gal}/F_{\rm A}$, where the true flux (in magnitudes) $m_{\rm A}$ differs from the contaminated flux through direct PSF fitting ($m_{\rm A+gal}$) in a quantity $F_{\rm gal}/F_{\rm A}$. This maximum contamination of A would be only of 40 mmag, and the real contamination of both components will be less than our upper limit. The artificial fluctuations (caused by variable contamination) will be even smaller than the typical contamination levels, so we expect they will not play an important role in analyses of quasar variability (e.g., time delay estimates).

In order to derive the light curves of the components A and B, we decided to use a direct PSF fitting method and do not consider the galaxy brightness in the fits. The key idea of this procedure was to obtain the different fluxes we were interested in by using a PSF that comes from a bright star in the field that is common to all frames. The point-like objects (quasar components and stars) are modelled by means of the empirical PSF. Hence, we do not use a theoretical PSF (i.e., Gaussian distribution, Lorentzian distribution, etc.), but the two-dimensional profile of a star in this field (a PSF star). Apart from a PSF star, we also need a reference star to do differential photometry and to obtain relative fluxes $m_{\rm A} - m_{\rm ref}$ and $m_{\rm B} - m_{\rm ref}$. The good behaviour of the reference star is usually checked by using a control star, so the fluxes $m_{\rm con} - m_{\rm ref}$ are expected to agree with a constant level. Nevertheless, since the R-band flux ratio is discussed in Sect. 5, we also want to obtain a rough estimation of the contaminations from this direct technique. With this aim, a deconvolution technique (Koptelova et al. 2005) is also applied to a set of frames with good seeing and signal. The selected frames are fitted to a model including the galaxy, and thus, we are able to obtain a few clean fluxes of components A and B and compare them with the corresponding contaminated fluxes (through a direct PSF fitting). The averaged contaminations are used in Sect. 5.

3.1. Calar Alto frames and light curves

We adopt a model of the system including two point-like sources and a constant background. The model is fitted to each image by adjusting its 7 free parameters (two-dimensional positions of A and B, instrumental fluxes of both components and background) to minimize the sum of the square residuals, as described in McLeod et al. (1998) and Lehár et al. (2000). We use windows of 64×64 pixel. Each empirical PSF is a subframe of 64×64 pixel around the PSF star (the "a" star in Fig. 1), while the lens system is analysed from a subframe of the same size, but centred on the double quasar. The instrumental fluxes of the "b", "c", "s1", and "s2" stars are also inferred from 64×64 pixel windows centred on them. We initially focus on the nearby field stars, and take the "b−c" stars as the control-reference objects. The "a" object is the brightest star in the "a−c" triangle, and "b" and "c" were spectroscopically identified by Kochanek et al. (1997) and Zickgraf et al. (2003): "b" is a FG star, whose spectrum includes the G-band and Ca II H−K lines, and "c" is an M 3 star. The $R-I$ and $B-R$ colours of the brightest component (A) and the "a" star are similar, the colours of the faintest component (B) are close to the colours of the "b" star, and the "c" star has colours different to those of the components and the "a−b" stars (see Table 1 of Kochanek et al. 1997). On the other hand, after checking the PSFs of the three nearby field stars ("a−c"), we do not find significant differences between them. This suggests that the global shape of the PSFs around the lens system does not depend on the position and colour of the point-like objects, so the PSF of the "a" star seems to be a reliable tracer of the PSF associated with any point-like object in the region of interest.

As a first attempt to obtain light curves, we use the "b" and "c" stars as the control and reference objects, respectively. Unfortunately, we find clear evidence of variability of the "c" star, since the three curves $m_{\rm A} - m_{\rm c}$, $m_{\rm B} - m_{\rm c}$ and $m_{\rm b} - m_{\rm c}$ have a similar global behaviour. This fact forces us to rule out the "c" star as a reference-control object and, thus, to take the "a" and "b" nearby field stars as the control and reference point-like sources, respectively. In the next subsection, we analyse the Maidanak-Wise fluxes $m_{\rm a} - m_{\rm b}$ and show that both stars ("a" and "b") are non-variable objects. This result guaranties the good behaviour of "b". The Calar Alto fluxes $m_{\rm a} - m_{\rm b}$ are not included in the analysis, since most Calar Alto data disagree with the Maidanak-Wise common level of flux. We found an anomaly in the behaviour of the Calar Alto relative fluxes for widely separate stars (see below), so only the relative fluxes for neighbouring point-like objects are reliable photometric measurements. Fortunately, the comparison between the quasar components and the "b" nearby reference star seems to be a feasible approach.

After applying the photometric method to the three individual frames for each filter and night (see Table 1), we obtain three different measurements of $y_{\rm A} = m_{\rm A} - m_{\rm b}$ and $y_{\rm B} = m_{\rm B} - m_{\rm b}$ in the V and R passbands for each night. To test the reliability of the instrumental fluxes of A and B, we analyse the residues in each residual frame. A residual frame is an image after subtracting the fitted background and point-like objects (PSF fitting method). More properly, we focus on the residual subframe occupied by the system, and then we estimate the residue-to-signal ratio (R/S) in each pixel of interest. An R/S value less than 10% is acceptable, so a subframe with at least 90% of the pixels having acceptable residues is considered to be related to reliable photometric solutions. Thus, we classify the individual fits in two categories: fits leading to <90% of pixels having acceptable residues (bad fits, unreliable results) and good fits that are associated with reliable results (≥90% of pixels having acceptable residues). As a complementary test, we study the relation between the quality of the fits (in terms of post-fit residues) and two relevant parameters (image quality). The signal-to-noise at the brightest pixel of the lens system, $(S/N)_{\rm max}$, and the seeing, $FWHM$ (in $''$), are the two parameters to compare with the fit quality. Some kind of correlation between good fits and good images is expected. In Fig. 3 we draw the $(S/N)_{\rm max}$−$FWHM$ plots for frames in the R filter (top panel) and the V filter (bottom panel). Circles and triangles represent good and bad fits, respectively. The plots in Fig. 3 indicate that the good fits correspond to images with high or moderate $(S/N)_{\rm max}$ (≥30). Moreover, at moderate $(S/N)_{\rm max}$ (∼30−50), most of the good fits seem to be associated with a relatively good seeing (<2$''$). To obtain robust photometry, we finally discard the frames corresponding to the triangles in Fig. 3. For each filter and night, if there are two or three good frames (good fits), then we get mean values of $y_{\rm A}$ and $y_{\rm B}$, and compute standard deviation of means as errors. We only consider relative fluxes with uncertainties ≤40 mmag.

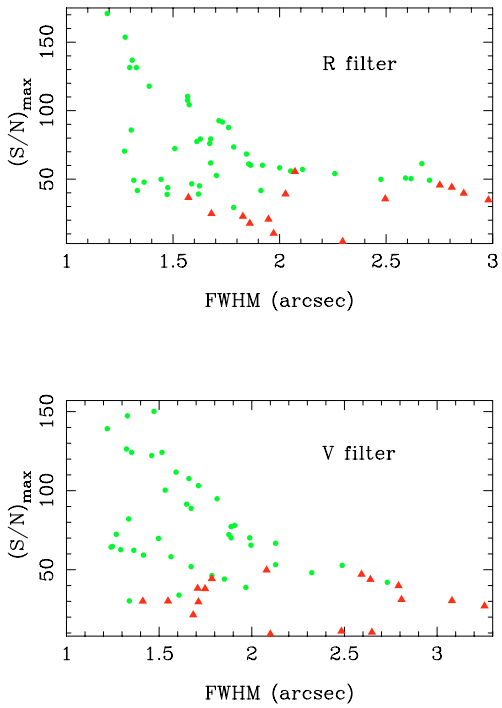

Fig. 3. $(S/N)_{\max}$ versus *FWHM* for the Calar Alto frames in the *R* filter (*top panel*) and the *V* filter (*bottom panel*). The circles and triangles represent the frames with good and bad post-fit residues, respectively (see main text).

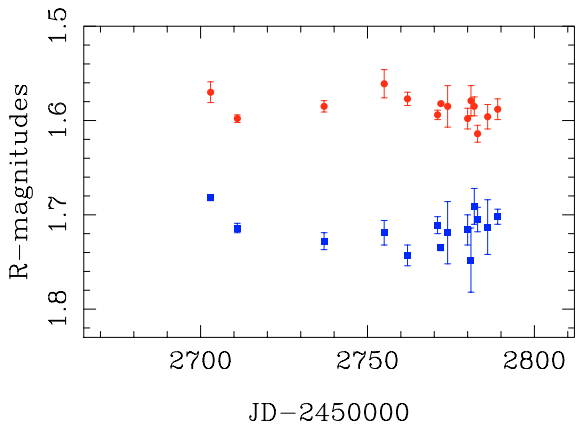

Fig. 4. Calar Alto light curves of the double quasar in the *R* filter. We use the "b" star as the reference object, because it is confirmed as a non-variable star in Fig. 7. The circles are the fluxes y_A ($y_A = m_A - m_b$) and the squares are the fluxes $y_B - 0.45$ mag ($y_B = m_B - m_b$). The A light curve has a final decline, while the B light curve ends in a rise.

Now we plot y_A (circles) and $y_B - 0.45$ mag (squares) in Fig. 4 (*R*-band fluxes). If we concentrate our attention on the period with the best sampling (after day 2755), the A light curve shows a moderate decline and the B record shows a moderate rise. Indeed, it seems that the "b" star is a good reference object (constant flux), since there is no zero-lag global correlation between y_A and y_B. In Fig. 5 we show the light curves y_A and $y_B - 0.65$ mag in the *V* passband. In this case we have a total of 11 points for the A component (circles) and 10 points for the B component (squares). The *V*-band and *R*-band light curves of the A component are consistent with each other. A final moderate decline appears in both curves. The situation is more confused for the B component. The *R*-band final rise is not clearly

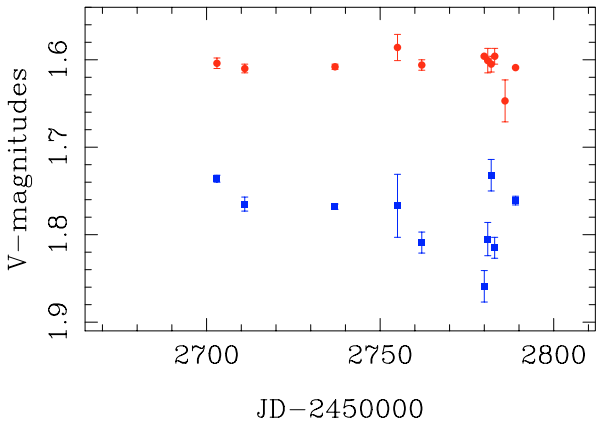

Fig. 5. Calar Alto light curves of the double quasar in the *V* filter. We use the non-variable star "b" as reference object (see Fig. 7). The circles are the fluxes y_A and the squares are the fluxes $y_B - 0.65$ mag.

reproduced in the *V* band, and the *V*-band final measurements could have underestimated formal errors. We note the relative faintness of B in the *V* band ($\Delta m \sim 0.8$ mag), and thus the possibility of systematic uncertainties when the PSF fitting method is applied at some epochs. The data in both optical filters are available at `http://grupos.unican.es/glendama/`.

After presenting the records of the double quasar, we concentrate on the Calar Alto light curves of the field stars that were previously introduced by Kochanek et al. (1997) and Nakos et al. (2003), i.e., $y_a = m_a - m_b$, $y_c = m_c - m_b$, $y_{s1} = m_{s1} - m_b$, and $y_{s2} = m_{s2} - m_b$. There are no previous studies on the variability of the nearby field stars "a–c". On the other hand, the farther field stars ("s1–s2") were verified as non-variable by using 76 Wise frames taken from December 24, 1999 to March 3, 2002 (Nakos et al. 2003). As Nakos et al. (2003) found that "s1" and "s2" seem to be useful reference stars, we check the behaviour of "s1–s2" in 2003. The PSF of the stars in the surroundings of the double quasar could differ slightly from the PSF of the "s1–s2" stars in a relatively far region. Therefore, we must be careful when obtaining the instrumental fluxes of the farther stars. To detect possible anomalies caused by a mismatch between the brightness profile of the "a" star and the PSF of "s1–s2", the light curves y_{s1} and y_{s2} are derived from both PSF fitting and aperture methods.

The records y_a, y_c, y_{s1}, and y_{s2} in the *R* filter are depicted in Fig. 6. To guide the eyes, we use some offsets and dashed horizontal lines and put all the relative records of each pair within a box. Filled and open symbols are associated with PSF fitting and aperture, respectively. The top box includes the y_a+2.15 mag fluxes (open squares). The second, third, and fourth boxes (under the top one) correspond to the y_c (filled squares), $y_{s1} + 2.38$ mag (filled and open triangles), and y_{s2}+0.29 mag (filled and open circles) records, respectively. As most of the stars are brighter than the quasar components (A and B) and they are far from other objects, the typical formal errors in the stellar fluxes are clearly less than the typical uncertainties in the fluxes of the components (usually fainter and are placed in a crowded region). The stellar error bars in Fig. 6 are often smaller than the sizes of the associated symbols.

When doing aperture photometry on six *R*-band Wise frames covering the first semester of 2003, we obtain a $y_a + 2.15$ mag light curve (open triangles in the top box of Fig. 6) that disagrees with the Calar Alto trend in the overlap period (between days 2710 and 2760). In the next subsection, we show that the

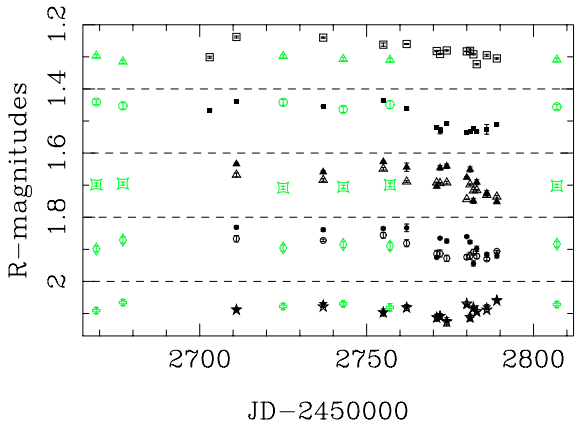

Fig. 6. Calar Alto light curves of the stars in the *R* filter. The Calar Alto fluxes are checked from six Wise frames. Filled and open symbols are associated with PSF fitting and aperture, respectively. First, the non-variable star "b" (see Fig. 7) is taken as the reference object. The top box incorporates the behaviour of $y_a + 2.15$ mag ($y_a = m_a - m_b$): Calar Alto (open squares) and Wise (open triangles). The second box (under the top box) contains the fluxes y_c ($y_c = m_c - m_b$): Calar Alto (filled squares) and Wise (open circles). The third and fourth boxes include the $y_{s1} + 2.38$ mag ($y_{s1} = m_{s1} - m_b$) and $y_{s2} + 0.29$ mag ($y_{s2} = m_{s2} - m_b$) records, respectively. In the third box: Calar Alto (filled and open triangles) and Wise (open astroids); in the fourth box: Calar Alto (filled and open circles) and Wise (open rhombuses). Second, we plot the $m_{s2} - m_{s1} - 0.20$ mag records in the bottom box: Calar Alto (filled and open star symbols) and Wise (open crosses).

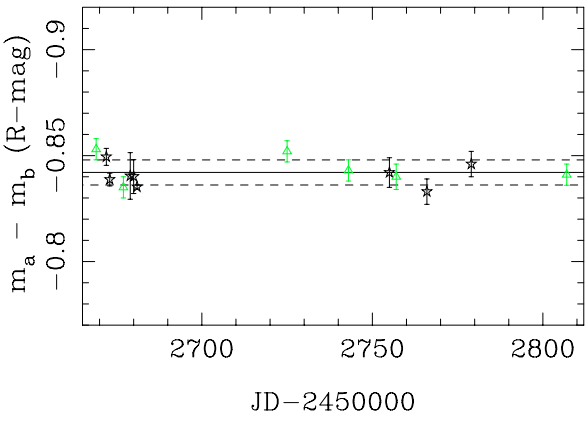

Fig. 7. Maidanak (open star symbols) and Wise (open triangles) light curves y_a in the *R* filter (from late January to the middle of June 2003). The solid line represents the global mean value and the two dashed lines describe the rms fluctuation of the measurements. This rms variation agrees with the typical uncertainty, so "a" and "b" seem to be non-variable sources.

Wise and Maidanak brightnesses are constant and consistent with each other, so the Calar Alto values of y_a are not true fluxes, but anomalous results. On the contrary, the Wise light curve y_c (open circles in the second box of Fig. 6) agrees with the Calar Alto curve in the overlap period. From the Wise frames we confirm the flux level during the high-state of "c". Unfortunately, the small-amplitude variability of "c" (rms fluctuation of ∼8 mmag) cannot be confirmed from the Wise data. The rms fluctuation of the Wise fluxes (∼9 mmag) is very similar to the Calar Alto variation, but the formal errors are relatively large (∼10 mmag). Moreover, there are no Wise frames in May 2003 (around the day 2780) and, thus, we cannot check (via Wise data) the reliability of the Calar Alto dip in y_c (80−100 mmag). However, the flux of the "c" star at day 2793 in the *V* band confirms the existence of a transition from the low-state to the high-state, which is finished at days 2800−2810 (see the last open circle in the second box of Fig. 6).

For the "s1–s2" stars, which are as far from star "b" as star "a" is, we again find a disagreement between the Calar Alto trends and the Wise records (open astroids and rhombuses in the third and fourth boxes of Fig. 6). Although aperture curves are closer to the Wise behaviours, we cannot reproduce the Wise data fairly. Some probes with the "x" star (using $y_x = m_x - m_b$) also indicate that the Calar Alto and Wise behaviours disagree. It seems that the differential photometry between widely separate stars may lead to meaningless results, and only the relative fluxes for neighbouring objects are reliable. To test this conclusion, apart from the successful results through the neighbouring stars "b" and "c", we also analyse the differential photometry between the pair "s1−s2" (see Fig. 1). The curves $m_{s2} - m_{s1} - 0.20$ mag are depicted in the bottom box of Fig. 6: Calar Alto (filled and open star symbols) and Wise (open crosses). In the overlap period (from day 2710 to day 2760), there is reasonable agreement between the results from both observatories, and the Calar Alto measurements seem to be quite reliable. From the Calar Alto frames, both photometric techniques are consistent with each other, but a constant flux cannot explain the observations. When we fit the data sets to a constant, our best solutions are characterised by $\chi^2 \sim 162$ (PSF fitting) and $\chi^2 \sim 6$ (aperture). It is a curious fact that aperture photometry on only one frame per night leads to relative fluxes in rough agreement with a constant level. However, more refined measurements (aperture or PSF fitting on several frames per night) reveal the variability of one ("s1" or "s2") or both stars.

3.2. *Maidanak frames and global R-band light curves of SBS 0909+532*

In the case of the *R*-band Maidanak observations, in order to derive the relative fluxes of the components of SBS 0909+532, we also use a direct PSF fitting. For a given frame, after obtaining a first estimate of the free parameters (initial solution), the fit is refined through an iterative procedure, which works as the CLEAN algorithm (Østensen 1994). The iterative task is done with each individual image, and the solutions converge after a few cycles. For each night, we take all the available images and obtain the mean values of y_A and y_B. From the standard deviation of the means, we also derive the errors in y_A and y_B. In agreement with the criteria in Sect. 3.1, only fluxes with errors less than or equal to 40 mmag are considered. Apart from the analysis of the lens system, using aperture photometry, we also measure y_a. The relative fluxes y_a are depicted in Fig. 7 (open star symbols). The Maidanak measurements in the first semester of 2003 and the six Wise data of y_a (open triangles; see here above) are tightly distributed around −0.842 mag (solid line in Fig. 7). The rms fluctuation of the data is only ∼6 mmag (see the dashed lines in Fig. 7), which is consistent with the typical error of the measurements. The y_a results in Fig. 7 suggest that both "a" and "b" are non-variable objects. Through 2003 (first and second semesters), we did not find any evidence in favour of variability of the "a−b" stars.

We show our global *R*-band light curves of SBS 0909+532 in Fig. 8. The open circles (Maidanak) and filled circles (Calar Alto) are the measurements of y_A, while the open squares (Maidanak) and filled squares (Calar Alto) are the values of $y_b - 0.45$ mag. We have 31 points for the A component

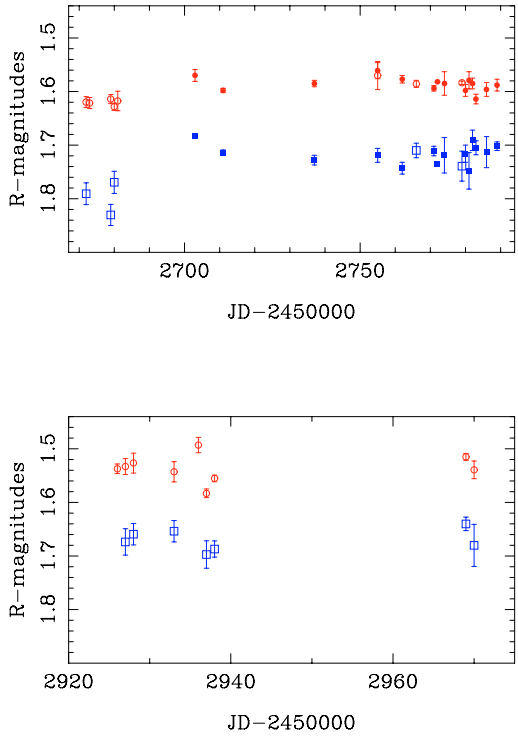

Fig. 8. Global R-band fluxes of SBS 0909+532 in 2003. The open circles (Maidanak) and filled circles (Calar Alto) are the fluxes y_A, whereas the open squares (Maidanak) and filled squares (Calar Alto) are the relative fluxes $y_B - 0.45$ mag. The top panel contains the results from early February to late May 2003 and the bottom panel includes the results from the middle of October to late November 2003.

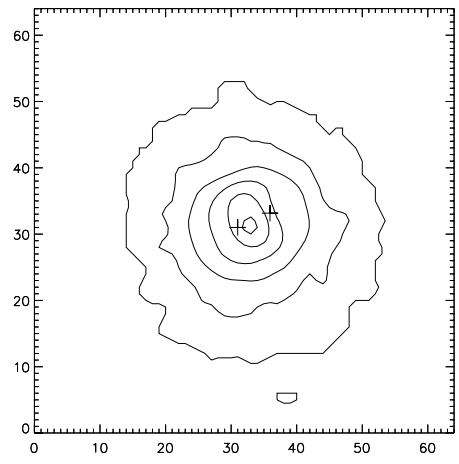

Fig. 9. Galaxy reconstruction obtained from selected Maidanak frames. Although the double quasar has been subtracted here, the positions of the components are labeled with two crosses: A is on the left and B is on the right, and the separation between both crosses is of 1.″1−1.″2. The galaxy contours cover a region of 10″ × 10″.

(circles) and 26 points for the B one (squares). The top panel of Fig. 8 contains the results from early February to late May 2003 and the bottom panel of Fig. 8 includes the results from the middle of October to late November 2003. For each component we test the existence of a bias between the Calar Alto and Maidanak fluxes, e.g., $\beta_A = y_A$ (Calar Alto) − y_A (Maidanak). Very small biases of $\beta_A = +15$ mmag and $\beta_B = -30$ mmag are found, and these corrections are taken into account to get the overall records in Fig. 8. The biases are derived from the comparison between the Maidanak fluxes in a thirty day period (from day 2750 to day 2780) and the Calar Alto fluxes at equal or close dates (see the top panel of Fig. 8).

To roughly estimate contaminations from the direct PSF fitting technique, we take some of our best Maidanak images (in terms of seeing conditions, $FWHM \sim 1''$) in the R band. A zoom-in of one of these best frames is shown in Fig. 2. First, we combine the selected frames and derive a numerical model of the galaxy from a regularizing algorithm. To produce a stabler reconstruction, the real galaxy profile is assumed to be close to the Sersic profile (Koptelova et al. 2005). Our deconvolution method differs only slightly from the former deconvolution techniques by Magain et al. (1998) and Burud et al. (1998). Figure 9 presents the galaxy reconstruction obtained from the stack of the R-band selected frames. The box in Fig. 9 is 16.″6 on a side. The positions of the components are labeled with two crosses: A is on the left and B is on the right. The innermost contours are circular-elliptical rings, whereas the outermost contours show a less definite shape. Secondly, the selected frames are fitted to a photometric model that includes the galaxy brightness. Therefore, we are able to infer clean relative fluxes of A and B (without contamination by galaxy light) and to compare them with the contaminated ones (from direct PSF fitting). As result of the comparison, we report typical (averaged) contaminations of 18.8 mmag and 4 mmag for the A and B components, respectively. These very weak contaminations are in reasonable agreement with our preliminary considerations in the beginning of this section and are taken into account in the measurement of the R-band flux ratio in Sect. 5.

4. Time delay

To calculate the time delay between both components of SBS 0909+532, we use the R-band brightness records from early February to late May 2003. The R-band records are more densely populated than the V-band ones. Moreover, the R-band time coverage from early February to late May 2003 (about 120 days) is longer than the time coverage from the middle of October to late November 2003 (about 50 days). Thus we focus on the R-band data from day 2670 to day 2790, i.e., 22 points in the A component and 19 points in the B component (see the top panel of Fig. 8). There are a different number of points for component A and component B because we only consider fluxes with uncertainties below 40 mmag (see Sect. 3). As the B component is fainter, its photometric uncertainties are larger and the number of final data is smaller. The new light curves are characterized by a mean sampling rate of one point every six days.

Once we have the data set, a suitable cross-correlation technique is required. Here we mainly use the χ^2 minimization (e.g., Kundić et al. 1997) and the minimum dispersion (D^2) method (Pelt et al. 1994, 1996). However, although other techniques are probably less robust than the χ^2 and D^2 ones (doing a first delay measurement without a previous empirical determination), we also tentatively explore the modified cross-correlation function (MCCF) technique (Beskin & Oknyanskij 1995; Oknyanskij 1997). The MCCF combines properties of both standard cross-correlation functions: the CCF by Gaskell & Spark (1986) and the DCF by Edelson & Krolik (1988). We begin our analysis using the χ^2 method, which is based on a comparison between the light curve y_A (or y_B) and the time shifted light curve y_B (or y_A). For a given lag, one can find the magnitude offset that minimizes the χ^2 difference. From a set of lags, a set of minima of χ^2 can be derived that permits us to make an χ^2 spectrum: χ^2 vs. lag.

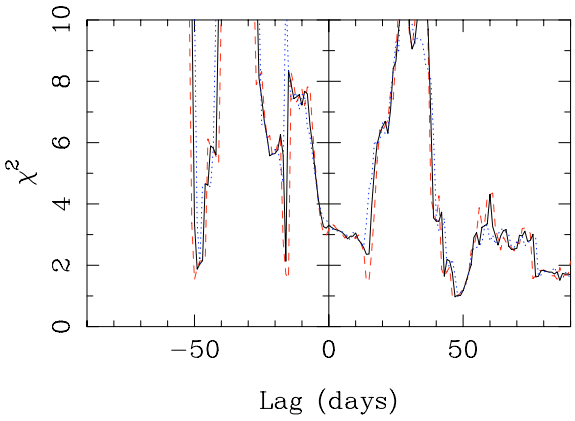

Fig. 10. χ^2 spectra for α = 7 days (dashed line), α = 8 days (solid line), and α = 9 days (dotted line). The parameter α is the semiwidth of the bins in the A component, so the three spectra represent different results of a cross-correlation with reasonable time-resolution (the mean sampling time is 6 days/point).

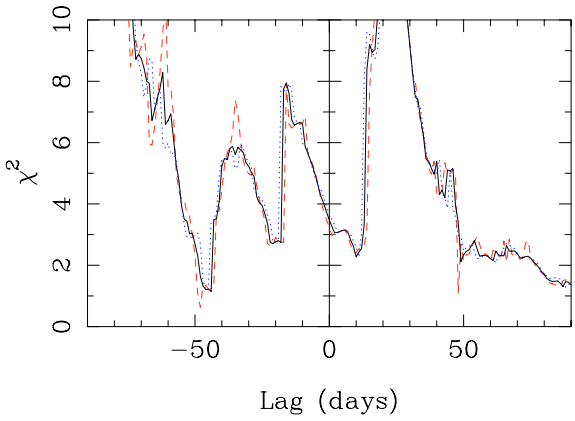

Fig. 11. χ^2 spectra for α = 9 days (dashed line), α = 10 days (solid line), and α = 11 days (dotted line), where α is the semiwidth of the bins in the B component.

The best solution to the delay is the lag corresponding to the minimum of the χ^2 spectrum. In general, the shifted epochs t'_B (or t'_A) do not coincide with the unchanged epochs t_A (or t_B), so we estimate the values of $y_A(t'_B)$ (or $y_B(t'_A)$) by averaging the A (or B) fluxes within bins centred on times t'_B (or t'_A) with a semiwidth α. To average in each bin, the use of weights is appropriate depending on the separation between the central time t'_B (or t'_A) and the dates t_A (or t_B) in the bin. In principle, we concentrate on the interval [−90, +90] days, which includes the predicted negative delays (see Introduction), as well as a wide range of unlikely positive delays (inconsistent with basic observations of the system).

First, the curve y_A and the time-shifted curve y_B are compared (using bins in the A component). In order to work with a reasonable time resolution, we use α values less than or equal to two times the mean sampling time, i.e., $\alpha \leq 12$ days. The χ^2 value roughly grows with the size of the bin, and $\chi^2 \sim 1$ for α = 7−9 days. For α = 7−9 days, there are best solutions $\Delta\tau_{BA}$ = +46−48 days (χ^2 = 0.97−0.98), and we show the corresponding spectra in Fig. 10. We have drawn together the spectra for α = 7 days, α = 8 days, and α = 9 days. Apart from the main minima close to +50 days, there are other secondary minima at negative and positive lags. In Fig. 10, two secondary minima seem to stay significant for all the bin sizes: the minima close to −50 days and the probable edge effects at +80−90 days. We also compare the curve y_B and the time shifted curve y_A, using bins in the B component. For α = 10 days, we obtain a best solution $\Delta\tau_{BA}$ = −44 days (χ^2 = 1.15). Smaller and larger bins lead to solutions characterised by $\chi^2 < 0.7$ and $\chi^2 \geq 1.2$, respectively. In Fig. 11, the solid line represents the spectrum for α = 10 days, while the dashed line represents the spectrum for α = 9 days, and the dotted line traces the spectrum for α = 11 days. Main minima in the interval of −40−50 days appear in all these cases. Unfortunately, important signals at positive lags and probable border effects at +80−90 days are again included in the complex spectra. The important structures at positive lags in Figs. 10, 11 are probably caused by artifacts in the cross-correlation, so they have no physical origin, but are due to the 10/20-day gaps and the moderate variability of the components. Therefore, taking α = 10 days (bins in the B component) and a negative range [−90, 0] days, we try to determine a pre-conditioned time delay.

In order to derive uncertainties, we follow a simple approach. We make one repetition of the experiment by adding a random quantity to each original flux in the light curves. The random quantities are realisations of normal distributions around zero, with standard deviations equal to the errors of the fluxes. We can make a large number of repetitions, and thus obtain a large number of $\Delta\tau_{BA}$ values. The true value will be included in the whole distribution of measured delays. From the χ^2 minimization (bins in B and α = 10 days) and 1000 repetitions, we obtain the histograms in Fig. 12. The main features of the distributions in the top panel (delays) and bottom panel (flux ratios) of Fig. 12 lead to measurements $\Delta\tau_{BA} = -45^{+1}_{-11}$ days and $\Delta m_{BA} = 0.590 \pm 0.014$ mag (95% confidence intervals). We note that the main delay peak is asymmetric, so 55% of the repetitions

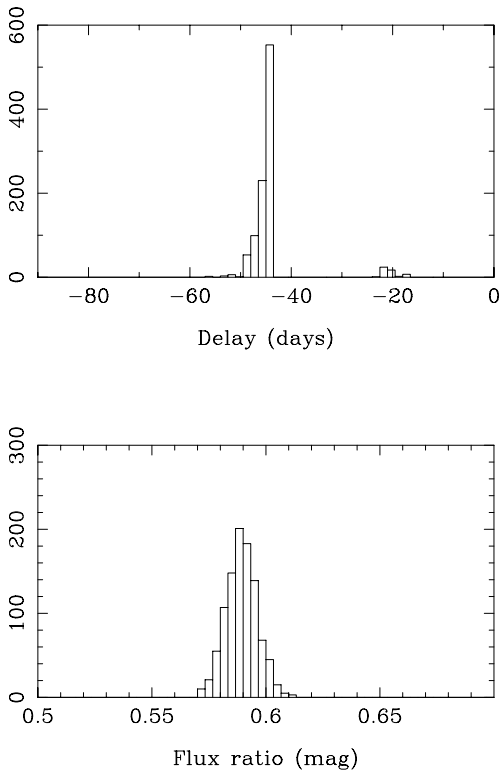

Fig. 12. Histograms from 1000 repetitions and the χ^2 minimization (bins in B and α = 10 days). *Top panel*: best solutions of the time delay. *Bottom panel*: best solutions of the magnitude offset (flux ratio). These distributions are consistent with a delay of about one and a half months and a time-delay-corrected flux ratio of about 0.59 mag.

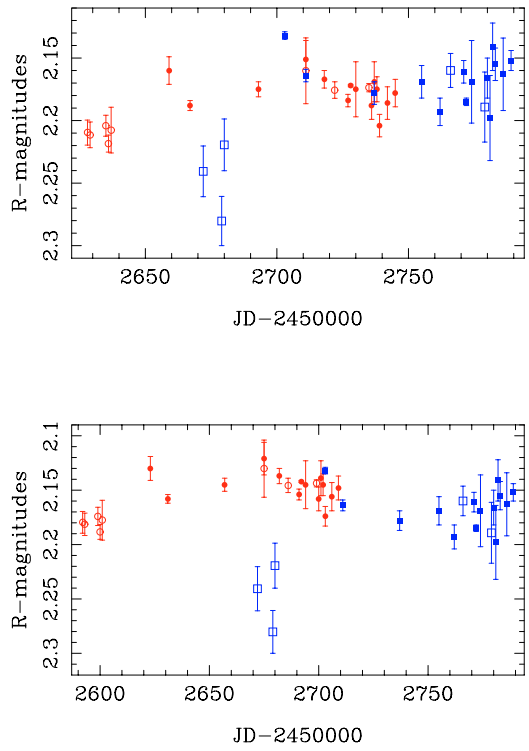

Fig. 13. Comparison between the shifted A light curve (circles) and the B light curve (squares). We use an χ^2 minimization, bins in B, and $\alpha = 10$ days. *Top panel*: best solution ($\Delta\tau_{BA} = -44$ days, $\Delta m_{BA} = 0.59$ mag). *Bottom panel*: solution for $\Delta\tau_{BA} = -80$ days ($\Delta m_{BA} = 0.56$ mag).

correspond to −44−45 days, whereas 40% of the repetitions correspond to values <− 45 days. The secondary delay peak (around −20 days) represents about 5% of the repetitions and is associated with the secondary minima in the negative region of Fig. 11. Therefore, the distribution in the top panel of Fig. 12 permits a 95% estimation of the time delay of SBS 0909+532.

In Fig. 13 (top panel), the A light curve, shifted by the optimal values of the time delay and the magnitude offset (time-delay-corrected flux ratio), and the unchanged B light curve are plotted. The cross-correlation using bins in the B component ($\alpha = 10$ days) indicates that the initial variations in the brightness of B reasonably agree with the final fluctuations in the brightness of A. The overlap for a delay of −80 days (e.g., Saha et al. 2006) also appears in the bottom panel of Fig. 13. However, this last time delay is clearly rejected by the observations, since the χ^2 value is higher than 10 ($\chi^2 \sim 18$).

To confirm the results from the χ^2 minimization, we also use the dispersion spectra introduced by Pelt et al. (1994, 1996). The basic idea is a combination of y_A and y_B into one global record for every lag τ and magnitude offset m_0 by taking all the values of y_A as they are and shifting the values of $y_B - m_0$ by τ. For each τ one can find the m_0 value that minimizes a dispersion estimate $D^2(\tau, m_0)$, so a dispersion spectrum $D^2(\tau)$ can be made in a direct way. We focus on the $D^2_{4,2}$ spectra that are called D^2 for simplicity (see Pelt et al. 1996, for details). This technique incorporates a decorrelation length (δ), where δ plays a role similar to that of α in the χ^2 method. Considering reasonable values of δ (from 7 to 11 days, see here above), we are able to make some interesting spectra. In Fig. 14 we have plotted together the spectra for $\delta = 7$ days, $\delta = 9$ days, and $\delta = 11$ days. Although there are main minima in the interval −40−50 days, there are also significant signals at positive lags and probable

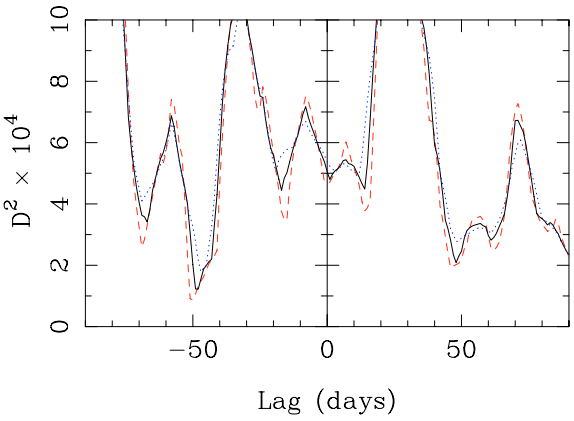

Fig. 14. Dispersion spectra for $\delta = 7$ days (dashed line), $\delta = 9$ days (solid line), and $\delta = 11$ days (dotted line). The parameter δ is the decorrelation length associated with the $D^2_{4,2}$ spectra (Pelt et al. 1996).

border effects at +90 days. In the negative region of Fig. 14, a secondary minimum around −70 days appears. Using $\delta = 9$ days and a negative range [−90, 0] days, we carry out a second preconditioned measurement of the time delay. The uncertainties are deduced from 1000 repetitions of the experiment (see here above), and the relevant histograms are shown in Fig. 15. While the top panel contains the distribution of delays, the bottom panel traces the distribution of flux ratios. Through the distributions in Fig. 15, we obtain $\Delta\tau_{BA} = -48^{+7}_{-6}$ days and $\Delta m_{BA} = 0.585 \pm 0.020$ mag (90% confidence interval). These D^2 results strengthen the conclusions from the χ^2 technique. A marginal measurement (10% confidence interval) of $\Delta\tau_{BA} = -67^{+1}_{-2}$ days and $\Delta m_{BA} = 0.558^{+0.007}_{-0.008}$ mag is also possible. However, both this possibility and the χ^2 result of around −20 days are probably related to the presence of gaps and the absence of strong variability in the light curves.

An MCCF technique (Beskin & Oknyanskij 1995; Oknyanskij 1997) is also explored. The MCCF is a modification of the standard cross-correlation functions (CCF and DCF). When this MCFF is applied to our data in the lag interval [−60, +60] days, the maximum correlation coefficient (0.907) corresponds to a lag of −45 days. This last result basically agrees with the χ^2 and dispersion spectra in Figs. 11 and 14.

5. Conclusions

Nowadays several groups are trying to coordinate the rich but scattered research potential in the field of gravitationally lensed quasar monitoring. The goals are to rationalize the astronomical work and to catalyze big scientific collaborations so that the astrophysics community can make a significant progress towards understanding the central engine in lensed quasars, the structure of the lensing galaxies, and the physical properties of the Universe as a whole. Some examples are the Astrophysics Network for Galaxy LEnsing Studies (ANGLES, `http://www.angles.eu.org/`), the Cosmic Lens All-Sky Survey (CLASS, `http://www.aoc.nrao.edu/~smyers/class.html`), and the COSmological MOnitoring of GRAvItational Lenses (COSMOGRAIL, `http://www.cosmograil.org/`). The University of Cantabria group (Spain), three groups of the former Soviet Union (Institute of Astronomy of Kharkov National University, Ukraine, Sternberg Astronomical Institute, Russia, and Ulug

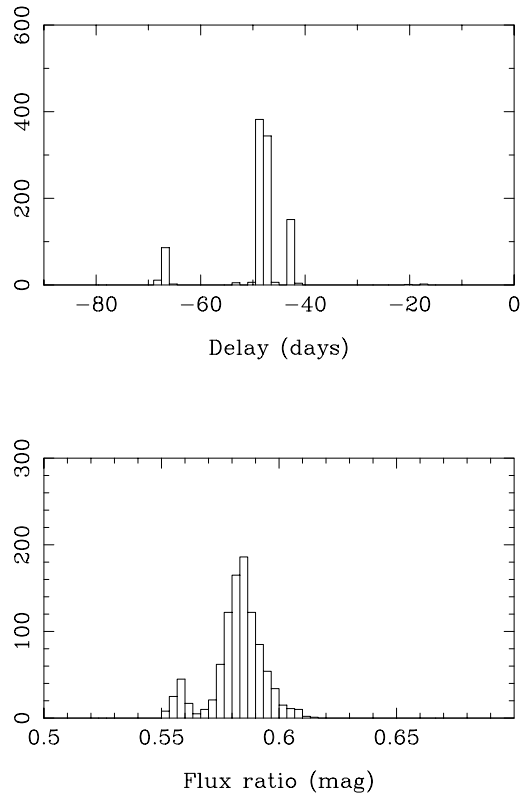

Fig. 15. Histograms from 1000 repetitions and the D^2 minimization (δ = 9 days). *Top panel*: best solutions of the time delay. *Bottom panel*: best solutions of the magnitude offset (flux ratio). These distributions are again consistent with a 1.5-month delay and and a time-delay-corrected flux ratio of about 0.58–0.59 mag.

Beg Astronomical Institute of Uzbek Academy of Science, Uzbekistan), and the Tel-Aviv University group (Israel) are also carrying out a series of initiatives to better exploit the recent individual monitoring campaigns, as well as to solidify some future common project. In this paper we present the first collaborative programme on the variability of the double quasar SBS 0909+532A,B. The *VR* observations of the system and the field stars were made with three modern ground-based telescopes in the year 2003.

The SBS 0909+532c star (N23210036195 in the GSC2.2 Catalogue) at (α, δ) = (09:12:53.59, +52:59:39.82) in J2000 coordinates is found to be variable, with two different levels of flux. The *VR* gap between the low state and the high state is 80−100 mmag, and the low-state lasts about one month. In the high state the star also seems to vary, but these small-amplitude variations are not as significant as the gap between states. We want to emphasise the variability of this nearby star ("c" star), and to encourage colleagues to follow-up its fluctuations and identify the kind of variable source. The "c" star cannot be used as the reference object (differential photometry), because it introduces a zero-lag global correlation between the light curves of the quasar components A and B. However, the "a–b" nearby stars are non-variable sources, and we choose the "b" star as the reference candle. On the other hand, the "s1" and "s2" stars are relatively far objects, which were proposed as good references in a previous analysis (Nakos et al. 2003). However, the new *R*-band light curve $m_{s2} - m_{s1}$ reveals the variability of one ("s1" or "s2") or both stars. This variability could be either a very rare phenomenon or a consequence of doing more refined measurements (aperture or PSF fitting on several frames per night). We warn about the possible problems with this pair of stars and think it merits more attention. The point-spread function (PSF) fitting methods permit the two components of the quasar to be resolved and the *VR* light curves of each component to be derived. These new *VR* light curves represent the first resolved brightness records of SBS 0909+532. Although the *V*-band curves are interesting, the *R*-band records seem more reliable and are more densely populated. The *R*-band curves show moderate variability through 2003, and the observed fluctuations are promising for different kinds of future studies.

To estimate the time delay between the components of SBS 0909+532, we use a 120-day piece of the *R*-band brightness records and χ^2 and dispersion (D^2) techniques. The cross-correlation of the two light curves (A and B) leads to complex χ^2 spectra. However, assuming that the quasar emission is observed first in B and afterwards in A, or in other words, $\Delta\tau_{BA} < 0$ (in agreement with basic observations of the system), 95% measurements $\Delta\tau_{BA} = -45^{+1}_{-11}$ days and $\Delta m_{BA} = 0.590 \pm 0.014$ mag are inferred from 1000 repetitions of the experiment (synthetic light curves based on the observed records). From the D^2 minimization (Pelt et al. 1996) and 1000 repetitions, we also obtain 90% measurements $\Delta\tau_{BA} = -48^{+7}_{-6}$ days and $\Delta m_{BA} = 0.585 \pm 0.020$ mag. The D^2 uncertainties are derived under the assumption already mentioned that $\Delta\tau_{BA}$ is negative. There is clear agreement between the results from both techniques, so a delay value of about one and a half months is strongly favoured. Our light curves rule out a delay close to three months, which has been claimed in a recent analysis (Saha et al. 2006). When we measure the time delay of the system, we simultaneously derive the time-delay-corrected flux ratio (at the same emission time) in the *R* band. This quantity, $\Delta m_{BA} = m_B(t + \Delta\tau_{BA}) - m_A(t)$, is contaminated by light of the lens galaxy; and taking the weak contaminations of A and B into account (see the end of Sect. 3.2), the totally corrected *R*-band flux ratio is 0.575 ± 0.014 mag. Our final *R* flux ratio is in total agreement with the rough (uncorrected by the time delay and the contamination by galaxy light) measurement by Kochanek et al. (1997): 0.58 ± 0.01 mag. To properly determine a flux ratio, one must use clean fluxes at the same emission time, i.e., fluxes at different observation times and without contamination (Goicoechea et al. 2005). Only for particular cases (e.g., faint lens galaxy, short delay, and moderate variability) may it be reasonable to use direct fluxes.

In order to get a reasonably good value of χ^2, we do not need to introduce a time-dependent magnitude offset or a complex iterative procedure (e.g., Burud et al. 2000; Hjorth et al. 2002), i.e., only a delay and a constant offset are fitted. This is a strong point of the analysis. The agreement between the results from different techniques is another strong point. However, the new measurements have some weak points that we want to comment on here. The weakest point is the relatively poor overlap between the A and B records, when the A light curve is shifted by the best solutions of the time delay and the magnitude offset (e.g., see the top panel of Fig. 13). Moreover, we carry out pre-conditioned measurements, since a negative interval [−90, 0] days is considered in the estimation of uncertainties (component B leading component A). This second weak point is related to the presence of 10/20-day gaps and the moderate variability of the components, which does not permit us to rule out positive delays fairly. We nevertheless note that the negative interval agrees with the predictions by Lehár et al. (2000) and Saha et al. (2006), and we find χ^2 and D^2 minima around −45 days when the observed data and both negative and positive lags are taken into account (see Figs. 11 and 14). Of course, as for any another

first determination of a time delay, the 1.5-month value should be confirmed by future studies.

Forty years ago, Refsdal (1964) suggested the possibility of determining the current expansion rate of the Universe (Hubble constant) and the masses of the galaxies from the time delays associated with extragalactic gravitational mirages. More recently, for a singular isothermal ellipsoid (SIE), Koopmans et al. (1998) found that the time delay can be cast in a very simple form, depending on basic cosmological parameters, redshifts and image positions. The relevant image positions are the positions with respect to the centre of the main lens galaxy, and the SIE delay is similar to the delay for a singular isothermal sphere (SIS). In principle, a singular density distribution is justified because a small core radius changes the time delay negligibly, and only a small core radius seems to be consistent with the absence of a faint central image (e.g., Kochanek 1996). Moreover, individual lenses and lens statistics are usually consistent with isothermal models (e.g., Witt et al. 2000, and references therein), so it is common to adopt an isothermal profile. Witt et al. (2000) show that an external shear changes the simple SIS time delay in proportion to the shear strength. For two-image lenses that have a small shear and images at different distances from the centre of the lens, the shear should have a small effect on the time delay. Thus, when one has accurate measurements of image positions, redshifts, and time delay, it is viable to accurately estimate H_0 (using complementary information on the matter/energy content of the Universe).

Very recently, Kochanek (2002) also presented a new elegant approach to the subject. He modelled the surface density locally as a circular power law, with a mean surface density $\langle\kappa\rangle$ in the annulus between the images. Expanding the time delay as a series in the ratio of the thickness of the annulus to its average radius, a delay is derived that is proportional to the SIS time delay. The zero-order expansion term consists of the SIS delay and a multiplicative factor $2(1-\langle\kappa\rangle)$. Kochanek also incorporated the quadrupoles of an internal shear (ellipsoid) and an external shear. However, for two-image lenses where the images lie on opposite sides of the lens, the delay depends little on the quadrupoles. This novel perspective is useful to infer $\langle\kappa\rangle$ from observations of the lens system (time delay, image positions, and redshifts) and complementary cosmological data (expansion and matter/energy content of the Universe).

For SBS 0909+532, although the redshifts are very accurately known and the time delay is now tightly constrained (or at least there is a first accurate estimation to be independently confirmed), the inaccurate position of the main lens galaxy does not permit an accurate measurement of the cosmic expansion rate and the surface density of the main deflector. We have $H_0 \propto \theta_B^2 - \theta_A^2$ and $1-\langle\kappa\rangle \propto (\theta_B^2 - \theta_A^2)^{-1}$, where θ_A and θ_B are the image angular positions with respect to the centre of the main lens galaxy. On the other hand, using the astrometry in Table 3 of Lehár et al. (2000), it is easy to obtain $\theta_B^2 - \theta_A^2 = 0.4 \pm 0.2$. Thus we conclude that the accuracy in $\theta_B^2 - \theta_A^2$ is only 50%, indicating the necessity of new accurate astrometry for SBS 0909+532.

Acknowledgements. The UC members are indebted to J. Alcolea (Observatorio Astronómico Nacional, Spain) for generously granting permission to operate the 1.52 m Spanish telescope at Calar Alto Observatory (EOCA) in March–June 2003. This 4-month season was supported by Universidad de Cantabria funds and the Spanish Department for Science and Technology grant AYA2001-1647-C02. A.U. thanks the Departamento de Física Teórica y del Cosmos de la Universidad de Granada (E. Battaner) for hospitality during the observational season. The post-observational work and the dissemination of results are supported by the Department of Education and Science grants AYA2002-11324-E, AYA2004-20437-E, and AYA2004-08243-C03-02. We acknowledge the use of data obtained by the SAI group headed by B. Artamonov. We are also indebted to D. Maoz and E. Ofek for providing the Wise frames of SBS 0909+532. A.P.Z. is grateful for the support of the Science and Technology Center of Ukraine (STCU), grant U127k. The observational work by the UBAI group (TA and OB) at Mt. Maidanak was supported by the German Research Foundation (DFG), grant 436 UZB 113/5/0-1. We are also grateful to the referee for several helpful comments. We acknowledge support by the European Community's Sixth Framework Marie Curie Research Training Network Programme, Contract No. MRTN-CT-2004-505183 "ANGLES". The GSC-II is a joint project of the Space Telescope Science Institute (STScI) and the Osservatorio Astronomico di Torino (OAT). STScI is operated by the Association of Universities for Research in Astronomy, for the NASA under contract NAS5-26555. The participation of the OAT is supported by the Italian Council for Research in Astronomy. Additional support is provided by ESO, Space Telescope European Coordinating Facility, the International GEMINI project, and the ESA.

References

Beskin, G. M., & Oknyanskij, V. L. 1995, A&A, 304, 341
Biggs, A. D., Browne, I. W. A., Helbig, P., et al. 1999, MNRAS, 304, 349
Burud, I., Stabell, R., Magain, P., et al. 1998, A&A, 339, 701
Burud, I., Hjorth, J., Jaunsen, A. O., et al. 2000, ApJ, 544, 117
Burud, I., Courbin, F., Magain, P., et al. 2002a, A&A, 383, 71
Burud, I., Hjorth, J., Courbin, F., et al. 2002b, A&A, 391, 481
Chartas, G. 2000, ApJ, 531, 81
Dai, X., Chartas, G., Agol, E., Bautz, M. W., & Garmire, G. P. 2003, ApJ, 589, 100
Edelson, R. A., & Krolik, J. H. 1988, ApJ, 333, 646
Fassnacht, C. D., Xanthopoulos, E., Koopmans, L. V. E., et al. 2002, ApJ, 581, 823
Gaskell, C. M., & Spark, L. S. 1986, ApJ, 305, 175
Gil-Merino, R., Wisotzki, L., & Wambsganss, J. 2002, A&A, 381, 428
Goicoechea, L. J. 2002, MNRAS, 334, 905
Goicoechea, L. J., Gil-Merino, R., & Ullán, A. 2005, MNRAS, 360, L60
Haarsma, D. B., Hewitt, J. N., Lehár, J., & Burke, B. F. 1999, ApJ, 510, 64
Hjorth, J., Burud, I., Jaunsen, A. O., et al. 2002, ApJ, 572, 11
Jakobsson, P., Hjorth, J., Burud, I., et al. 2005, A&A, 431, 103
Kochanek, C. S. 1996, ApJ, 466, 638
Kochanek, C. S. 2002, ApJ, 578, 25
Kochanek, C. S., Falco, E. E., Schild, R., et al. 1997, ApJ, 479, 678
Kochanek, C. S., Schneider, P., & Wambsganss, J. 2004, Part 2 of Gravitational Lensing: Strong, Weak & Micro, in Proc. of the 33rd Saas-Fee Advanced Course, ed. G. Meylan, P. Jetzer, & P. North (Berlin: Springer-Verlag)
Kochanek, C. S., Morgan, N. D., Falco, E. E., et al. 2005 [arXiv:astro-ph/0508070]
Koopmans, L. V. E., de Bruyn, A. G., & Jackson, N. 1998, MNRAS, 295, 534
Koopmans, L. V. E., de Bruyn, A. G., Xanthopoulos, E., & Fassnacht, C. D. 2000, A&A, 356, 391
Koptelova, E., Shimanovskaya, E., Artamonov, B., et al. 2005, MNRAS, 356, 323
Kundić, T., Turner, E. L., Colley, W. N., et al. 1997, ApJ, 482, 75
Lehár, J., Falco, E. E., Kochanek, C. S., et al. 2000, ApJ, 536, 584
Lovell, J. E. J., Jauncey, D. L., Reynolds, J. E., et al. 1998, ApJ, 508, L51
Lubin, L. M., Fassnacht, C. D., Readhead, A. C. S., Blandford, R. D., & Kundić, T. 2000, ApJ, 119, 451
Magain, P., Courbin, F., & Sohy, S. 1998, ApJ, 494, 472
McLeod, B. A., Bernstein, G. M., Rieke, M. J., & Weedman, D. W. 1998, AJ, 115, 1377
Mediavilla, E., Muñoz, J. A., Kochanek, C. S., et al. 2005, ApJ, 619, 749
Motta, V., Mediavilla, E., Muñoz, J. A., et al. 2002, ApJ, 574, 719
Nakos, Th., Ofek, E. O., Boumis, P., et al. 2003, A&A, 402, 1157
Ofek, E. O., & Maoz, D. 2003, ApJ, 594, 101
Oknyanskij, V. L. 1997, In Astronomical Data Analysis Software and Systems VI, ed. G. Hunt, & H. E. Payne, ASP Conf. Ser., 125, 162
Oscoz, A., Serra-Ricart, M., Mediavilla, E., Buitrago, J., & Goicoechea, L. J. 1997, ApJ, 491, L7
Østensen, R. 1994, Ph.D. Thesis, University of Tromsø
Ovaldsen, J. E., Teuber, J., Schild, R. E., & Stabell, R. 2003, A&A, 402, 891
Page, K. L., Reeves, J. N., O'Brien, P. T., Turner, M. J. L., & Worrall, D. M. 2004, MNRAS, 353, 133
Patnaik, A. R., & Narasimha, D. 2001, MNRAS, 326, 1403
Pelt, J., Hoff, W., Kayser, R., Refsdal, S., & Schramm, T. 1994, A&A, 286, 775
Pelt, J., Kayser, R., Refsdal, S., & Schramm, T. 1996, A&A, 305, 97
Refsdal, S. 1964, MNRAS, 128, 307
Saha, P., Courbin, F., Sluse, D., Dye, S., & Meylan, G. 2006, A&A, 450, 461
Schechter, P. L., Bailyn, C. D., Barr, R., et al. 1997, ApJ, 475, L85
Serra-Ricart, M., Oscoz, A., Sanchis, T., et al. 1999, ApJ, 526, 40
Stepanyan, D. A., Lipovetskii, V. A., Chavushyan, V. O., Erastova, L. K., & Shapovalova, A. I. 1991, Afz, 34, 1
Ullán, A. 2005, in e-Proceedings of the GLQ Workshop 25 Years After the Discovery: Some Topics on Lensed QSOs, http://grupos.unican.es/glendama/e-Proc.htm, C2
Ullán, A., Goicoechea, L. J., Muñoz, J. A., et al. 2003, MNRAS, 346, 415
Witt, H. J., Mao, S., & Keeton, C. R. 2000, ApJ, 544, 98
Wyrzykowski, L., Udalski, A., Schechter, P. L., et al. 2003, Acta Astron., 53, 229
Ziad, A., Gredel, R., Aceituno, J., et al. 2005, MNRAS, 362, 455
Zickgrof, F.-J., Engels, D., Hagen, H.-J., Reimers, D., & Voges, W. 2003, A&A, 406, 535